

Carbon-rich dust in comet 67P/Churyumov-Gerasimenko measured by COSIMA/Rosetta

Anaïs Bardyn, Donia Baklouti, Hervé Cottin, Nicolas Fray, Christelle Briois, John Paquette, Oliver Stenzel, Cecile Engrand, Henning Fischer, Klaus Hornung, et al.

▶ **To cite this version:**

Anaïs Bardyn, Donia Baklouti, Hervé Cottin, Nicolas Fray, Christelle Briois, et al.. Carbon-rich dust in comet 67P/Churyumov-Gerasimenko measured by COSIMA/Rosetta. Monthly Notices of the Royal Astronomical Society, 2017, 469 (Suppl_2), pp.S712-S722. 10.1093/mnras/stx2640 . insu-02764524

HAL Id: insu-02764524
https://insu.hal.science/insu-02764524

Submitted on 4 Jun 2020

HAL is a multi-disciplinary open access archive for the deposit and dissemination of scientific research documents, whether they are published or not. The documents may come from teaching and research institutions in France or abroad, or from public or private research centers.

L'archive ouverte pluridisciplinaire **HAL**, est destinée au dépôt et à la diffusion de documents scientifiques de niveau recherche, publiés ou non, émanant des établissements d'enseignement et de recherche français ou étrangers, des laboratoires publics ou privés.

Monthly Notices of the ROYAL ASTRONOMICAL SOCIETY
MNRAS **469,** S712–S722 (2017) doi:10.1093/mnras/stx2640

Carbon-rich dust in comet 67P/Churyumov-Gerasimenko measured by COSIMA/*Rosetta*

Anaïs Bardyn,[1,2★†‡] Donia Baklouti,[3★†] Hervé Cottin,[1★] Nicolas Fray,[1] Christelle Briois,[2] John Paquette,[4] Oliver Stenzel,[4] Cécile Engrand,[5] Henning Fischer,[4] Klaus Hornung,[6] Robin Isnard,[1,2] Yves Langevin,[3] Harry Lehto,[7] Léna Le Roy,[8] Nicolas Ligier,[3] Sihane Merouane,[4] Paola Modica,[1,2] François-Régis Orthous-Daunay,[9] Jouni Rynö,[10] Rita Schulz,[11] Johan Silén,[10] Laurent Thirkell,[2] Kurt Varmuza,[12] Boris Zaprudin,[7] Jochen Kissel[4] and Martin Hilchenbach[4]

[1]*Laboratoire Interuniversitaire des Systèmes Atmosphériques (LISA), UMR CNRS 7583, Université Paris-Est Créteil et Université Paris Diderot, Institut Pierre Simon Laplace, F-94000 Créteil, France*
[2]*Laboratoire de Physique et Chimie de l'Environnement et de l'Espace (LPC2E), CNRS/Université d'Orléans, F-45071 Orléans, France*
[3]*Institut d'Astrophysique Spatiale (IAS), CNRS/Université Paris Sud, Bâtiment 121, F-91405 Orsay, France*
[4]*Max-Planck-Institut für Sonnensystemforschung (MPS), Justus-von-Liebig-Weg 3, D-37077 Göttingen, Germany*
[5]*Centre de Sciences Nucléaires et de Sciences de la Matière (CSNSM), CNRS/IN2P3 – Université Paris Sud – UMR 8609, Université Paris-Saclay, Bâtiment 104, F-91405 Orsay Campus, France*
[6]*Universität der Bundeswehr LRT-7, Werner Heisenberg Weg 39, D-85577 Neubiberg, Germany*
[7]*Tuorla Observatory, Department of Physics and Astronomy, University of Turku, Väisäläntie 20, FI-21500 Piikkiö, Finland*
[8]*Center for Space and Habitability (CSH), University of Bern, Sidlerstrasse 5, CH-3012 Bern, Switzerland*
[9]*Institut de Planétologie et d'Astrophysique de Grenoble (IPAG), UMR 5274, Université Grenoble Alpes, CNRS, F-38000 Grenoble, France*
[10]*Finnish Meteorological Institute, Observation Services, Erik Palménin Aukio 1, FI-00560 Helsinki, Finland*
[11]*European Space Agency (ESA), Scientific Support Office, Keplerlaan 1, Postbus 299, NL-2200 AG Noordwijk, the Netherlands*
[12]*Institute of Statistics and Mathematical Methods in Economics, Vienna University of Technology, Wiedner Hauptstrasse 7/105-6, A-1040 Vienna, Austria*

Accepted 2017 October 6. Received 2017 September 11; in original form 2017 July 26

ABSTRACT

Cometary ices are rich in CO_2, CO and organic volatile compounds, but the carbon content of cometary dust was only measured for the Oort Cloud comet 1P/Halley, during its flyby in 1986. The COmetary Secondary Ion Mass Analyzer (COSIMA)/*Rosetta* mass spectrometer analysed dust particles with sizes ranging from 50 to 1000 μm, collected over 2 yr, from 67P/Churyumov-Gerasimenko (67P), a Jupiter family comet. Here, we report 67P dust composition focusing on the elements C and O. It has a high carbon content (atomic $C/Si = 5.5\ ^{+1.4}_{-1.2}$ on average) close to the solar value and comparable to the 1P/Halley data. From COSIMA measurements, we conclude that 67P particles are made of nearly 50 per cent organic matter in mass, mixed with mineral phases that are mostly anhydrous. The whole composition, rich in carbon and non-hydrated minerals, points to a primitive matter that likely preserved its initial characteristics since the comet accretion in the outer regions of the protoplanetary disc.

Key words: astrochemistry – space vehicles: instruments – techniques: miscellaneous – comets: general – comets: individual: 67P/Churyumov-Gerasimenko.

1 INTRODUCTION

Comets were accreted during the early stage of the formation of the Solar System. Because of their small size and their accretion in a cold environment far from the Sun, the composition of comets could reflect that of the early protosolar nebula where they were formed (Willacy et al. 2015). They are thus expected to contain more

★ E-mail: abardyn@carnegiescience.edu (AB); donia.baklouti@ias.u-psud.fr (DB); herve.cottin@lisa.u-pec.fr (HC)
† These authors contributed equally to this work.
‡ Present address: Department of Terrestrial Magnetism, Carnegie Institution of Washington, 5241 Broad Branch Road, Washington, DC 20015, USA.

© 2017 The Authors
Published by Oxford University Press on behalf of the Royal Astronomical Society

Downloaded from https://academic.oup.com/mnras/article-abstract/469/Suppl_2/S712/4670835 by CNRS user on 04 June 2020

light elements than the most primitive objects of the asteroid belt, the parent bodies of carbonaceous chondritic meteorites (Bell et al. 1989). In particular, a high concentration of carbon (close to the solar abundance) would be considered as evidence of a primitive material. The dust particles ejected from comet nuclei are therefore expected to be among the most pristine material within the Solar System, remaining almost unmodified and stored at low temperatures since their co-accretion with ices to form the icy bodies (Mumma & Charnley 2011).

Several past space missions have shed a first light on cometary dust composition. In 1986, the first *in situ* analyses of the Oort Cloud comet 1P/Halley dust particles with the Giotto, Vega 1 and Vega 2 missions revealed that they contain minerals and carbonaceous matter made of C, H, O and N atoms (Kissel et al. 1986a; Kissel et al. 1986b; Clark et al. 1987; Jessberger et al. 1988; Lawler & Brownlee 1992). Their overall composition was estimated to be close to the one of the solar photosphere for most of the measured elements. In particular, the atomic C/Si bulk ratio of 1P/Halley particles was estimated to be 4.4 ± 1.3 (Jessberger et al. 1988), almost six times the average C/Si ratio of 0.76 ± 0.10 found in CI carbonaceous chondritic meteorites and only less than twice to the protosolar abundance of 7.19 ± 0.83 (Lodders 2010). Twenty years later, the Stardust mission enabled the first laboratory analysis of samples brought back to Earth from 81P/Wild 2, a Jupiter family comet. One major finding was that the returned particles contained crystalline minerals (silicates mainly) that have been processed at high temperature in the inner parts of the protoplanetary disc (Brownlee 2014). However, a quantification of the carbonaceous materials in the particles of 81P/Wild 2 was not possible due to the high impact speed and collection method of these particles (Sandford et al. 2010; Brownlee 2014).

We report here the global composition, including for the first time carbon and oxygen abundance ratios, of the refractory phases of dust particles from the Jupiter family comet 67P/Churyumov-Gerasimenko (hereafter 67P), as deduced from the COmetary Secondary Ion Mass Analyzer (COSIMA) instrument measurements during the *Rosetta* mission. COSIMA is a Time-Of-Flight Secondary Ion Mass Spectrometer (TOF-SIMS) onboard the *Rosetta* orbiter. The determination of the elemental composition of comet 67P's dust is one of the main goals of the COSIMA instrument (Kissel et al. 2007). Two notable facts differentiate analyses with COSIMA from those of previous missions: (i) the *Rosetta* spacecraft followed comet 67P at close distances for a period of 2 yr; during this time, COSIMA collected more than 35 000 cometary particles and fragments thereof (Merouane et al. 2017), with sizes ranging from ∼10 to 1000 μm, and analysed *in situ* about 250 of them. Previous missions were flybys missions and thus could not spend more than a few hours near the cometary nuclei. (ii) The low impact velocity of the collected particles (<10 m s^{-1}; Rotundi et al. 2015) on the COSIMA targets preserved the dust chemical properties and part of its physical structure (e.g. the porosity of the particles; Hornung et al. 2016; Langevin et al. 2016). On the contrary, the Stardust space probe collected cometary particles at high velocity impact (6 km s^{-1}), which altered the samples to some extent and compromised the quantification and characterization of the less refractory material (the carbon content in particular; Sandford et al. 2010; Brownlee 2014). Giotto, Vega 1 and Vega 2 collected particles at even higher velocities (68, 79 and 77 km s^{-1}, respectively). This hypervelocity was directly used for the impact-ionization process of the mass spectrometers PIA, PUMA-1 and PUMA-2, but made it difficult at that time to have completely accurate quantitative results due to the lack of relevant ground calibration experiments (Jessberger et al. 1988).

2 METHODS

2.1 Instrument description

The COSIMA instrument is a TOF-SIMS that collected and analysed *in situ* cometary dust particles in the vicinity of comet 67P/Churyumov-Gerasimenko (Kissel et al. 2007). As stated before, the particles were collected at low impact velocity (<10 m s^{-1}; Rotundi et al. 2015) on a set of target plates, each of 10 × 10 mm^2 in size. All the particles considered in this study have been collected on target plates covered by a porous gold layer (Hornung et al. 2014). During the escort phase of the mission, which lasted more than 2 yr, the temperature within the instrument was about 283 K. Collected particles were first localized by an embedded microscope called COSISCOPE, which imaged the targets before and after exposure to the cometary dust in the near comet environment (Langevin et al. 2016). Selected particles were then analysed by SIMS. The primary ion beam was generated by a liquid indium ion source, with energy of 8 keV. The beam was pulsed (∼1000 ions per pulse within 3 ns with a 1.5 kHz repetition rate) and focused to give a footprint of 35 × 50 μm^2 (full-width at half-maximum) on the target. The primary $^{115}In^+$ ions impacted the solid sample and released secondary ions from the top surface layers by collision cascades. The secondary ions came from a few nanometres of the primary ion's impact area (Henkel & Gilmour 2014). These ions were then accelerated into a drift tube with an ion reflector, resulting in a mass spectrum of secondary ions on the detection system. The nominal mass resolution $m/\Delta m$ of COSIMA is about 1400 (full-width at half-maximum at $m/z = 100$; Hilchenbach et al. 2016), which enables in most cases, in this mass range, to distinguish elemental ions from hydrogen-bearing organic ions for a given integer mass. Positive and negative ion mass spectra were acquired on and near each analysed particle. Because the footprint of the primary ion beam can be comparable to the size of the particles, mass spectra can contain secondary ions from the particle, the target plate or both. To preserve the lifetime of the primary indium ion source of the instrument and to extend it for the whole 2 yr *Rosetta* mission, no sputtering was performed on samples before the analyses presented in this study. Sputtering is a current methodology in the sample analysis protocol in TOF-SIMS, but it is extremely costly in terms of primary ion source consumption. Each spectrum had an acquisition time of 2.5 min and corresponds to 225 000 individual primary ion beam shots. The mean current is estimated to be 7 nA cm^{-2}. For each analysis performed, two consecutive spectra were acquired at the same *X*- and *Y*-coordinates. A series of spectra could be measured at different coordinates on the same particle at a specific date. If the first analysis set was promising, the same particle could be analysed again as needed.

2.2 Selected dust particles

For this study, a set of 30 particles representative of a large range of sizes (area comprised between 0.7 × 10^4 μm^2 and 23 × 10^4 μm^2), typologies and collection times, before and after perihelion, has been selected for the high quality of their mass spectra and the ability to separate the spectra acquired on the particle from those measured on the nearby background (see Sections 2.4.1 and 2.4.2 for more details on the way the spectra are evaluated and selected). This selection is presented in Table 1. It lists 30 cometary particles that belong to the four typologies observed (Langevin et al. 2016) and their collection dates cover a wide time range (from December 2014 to March 2016). Some of them have also been analysed several times. In the negative mode of the instrument, 16 particles have been

Downloaded from https://academic.oup.com/mnras/article-abstract/469/Suppl_2/S712/4670835 by CNRS user on 04 June 2020

Table 1. Characteristics of the dust particles selected for this study.

Name	Target	Typology	Area (10^4 μm^2)	Collection period	Date(s) of analysis in positive mode	Date(s) of analysis in negative mode
Bonin (B.)	1CD	R	3.4 (*)	31/07/2015–01/08/2015	21/08/2015; 10/09/2015	–
Devoll (De.)	1CD	G	0.9 (*)	31/07/2015–01/08/2015	16/10/2015	–
Umeka (Um.)	1CD	G	1.02	03–04/07/2015	21/08/2015; 10/09/2015	–
André (An.)	1CF	G	2.62	09–14/01/2015	17/12/2015	16/12/2015
Elly (El.)	1CF	R	1.36	24–25/01/2015	17/12/2015	16/12/2015
Hase (H.)	1CF	R	1.64	24–25/01/2015	17/12/2015	16/12/2015
Isbert (I.)	1CF	R	2.8	28–29/01/2015	17/12/2015	16/12/2015
Alicia (Al.)	1CF	R	1.86	16–20/12/2014	11/12/2015	10/12/2015
Justus	1CF	G	5.92	28–29/01/2015		10/12/2015
Uli (Ul.)	1CF	C	1.66	20–27/12/2014	29/01/2016	10/12/2015
Atika (At.)	1CF	G	1.86	16–20/12/2014	17/12/2015; 03/02/2016	–
Günter	1D2	R	12.35	29/02–01/03/2016	–	14–15/04/2016
Amelie	1D2	R	6.10	16–18/11/2015	–	25/11/2015
Sophie	1D2	R	4.92	16–18/11/2015	–	25/11/2015
Juliette (Jul.)	1D2	G	2.39	23–29/10/2015	18/11/2015	18/11/2015
Fadil (F.)	1D2	G	1.63	16–18/11/2015	26/11/2015	–
Karen (Ka.)	2CD	S	13.80	25–26/07/2015	05/08/2015; 17/09/2015; 30/09/2015; 25/02/2016	–
Jean-Pierre (JP.)	2CF	S	9.5	24–25/01/2015	08/01/2016; 04/02/2016	–
Jessica (Je.)	2CF	S	23.2	26–27/01/2015	07/01/2016; 04/02/2016	–
Lari (L.)	2CF	S	1.96	24–25/01/2015	01/01/2016	–
Kenneth (Ke.)	2D1	R	4.53	11–12/05/2015	18/06/2015; 02/07/2015	17/06/2015
Roberto (R.)	2D1	S	0.7 (*)	11–12/05/2015	18/06/2015; 02/07/2015	17/06/2015
Francesco	2D1	R/G	12.07	11–12/05/2015	–	17/06/2015
David (Da.)	2D1	S	4.9 (*)	11–12/05/2015	13/06/2015; 23/12/2015	12/06/2015
Jakub (Ja.)	2D1	S	11.98	11–12/05/2015	21/05/2015; 13/06/2015	12/06/2015
Enako (En.)	2D1	S	1.1 (*)	11–12/05/2015	18/06/2015	–
Stefane (St.)	2D2	R	0.94	17–18/01/2016	11/02/2016	–
Juvenal (Juv.)	3C7	C	1.5	01–09/03/2015	13/11/2015	–
Matt (M.)	3CF	R	2.8	24–25/01/2015	13/01/2016; 05/02/2016	–
Sachi (Sa.)	3D1	C	0.78	11–12/05/2015	02/12/2015	–

Note. For each particle, the name, the collection target plate, the typology classification, the collection period and the dates of TOF-SIMS measurements in positive and/or negative modes are indicated. The typology of the particles refers to the classification established by Langevin et al. (2016): R, G, C and S stand for Rubble pile, Glued cluster, Compact particle and Shattered cluster, respectively. The area of the particles is calculated according to the method described in Langevin et al. (2016), except for the particles designed by (*) for which an estimation is given because the proximity of other particles makes it difficult to accurately discern their outlines.

selected and account for a total of 242 negative mass spectra. In the positive mode of the instrument, 25 particles have been selected and account for a total of 494 positive mass spectra.

2.3 Particle Atika as a reference for a typical cometary SIMS signature

TOF-SIMS analyses by COSIMA probed different areas of the collected particles: their surface after collection (some particles result from fragmentation of a larger parent before reaching the target; Langevin et al. 2016; Merouane et al. 2017) and their inner volume after the pulverization due to SIMS analyses. As an example, the COSISCOPE images of the particle Atika are displayed in Fig. 1. The sub-pixel image (a) was acquired on 2015 February 9, before the SIMS analysis, when its initial size was 170 × 115 × 85 μm^3. The image (b) was acquired on 2015 December 17 after the first negative SIMS analysis. It can be noted that the particle is fragmented into more smaller units, a phenomenon previously reported in Hilchenbach et al. (2016) and Hilchenbach et al. (2017). Further analyses were conducted until the last image (c) obtained on 2016 June 10. The final size of 250 × 160 × 30 μm^3 demonstrates the particle's fragmentation; its height loss, in particular. Its tensile strength is low enough (Hornung et al. 2016; Hilchenbach et al. 2017) so that the primary ions shatter the particle, without modifying the signature of its mass spectra after several analyses. Thus, experiments conducted on particles such as Atika have allowed to perform positive SIMS analyses on a freshly exposed cometary surface.

2.4 Data analysis

As stated above, due to the size of the ion beam, when analysing a cometary particle, the secondary ions are emitted most of the time from the particle itself but also from the surrounding target background. Therefore, it is essential to remove this non-cometary contribution from the spectra. The 2 yr of analyses with COSIMA have led to a good characterization of the cometary particle signature. A processing method has been established to retrieve the signal coming from the cometary particles for the positive and negative mass spectra.

2.4.1 Data analysis for positive mass spectra

TOF-SIMS is surface-sensitive instrument. Positive ion mass spectra from the target background of COSIMA are dominated by PolyDiMethylSiloxane (PDMS) polymers $(C_2H_6OSi)_n$, a common component measured in the background of TOF-SIMS experiments due to its high ionization yield even at very low concentrations (Henkel & Gilmour 2014). Its positive mode mass spectrum is characterized by a specific fingerprint, in which the highest

Downloaded from https://academic.oup.com/mnras/article-abstract/469/Suppl_2/S712/4670835 by CNRS user on 04 June 2020

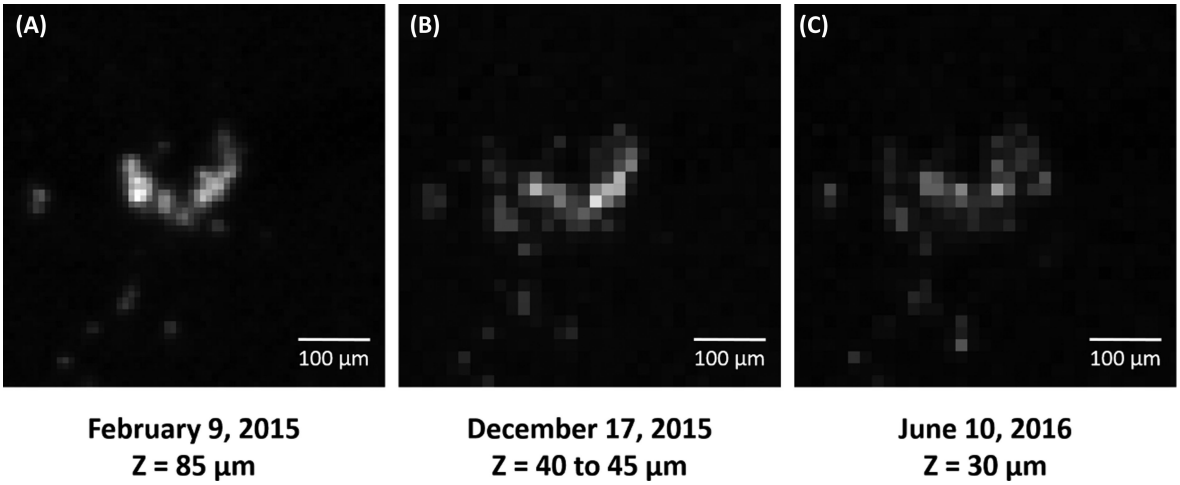


Figure 1. Optical images of particle Atika taken at different dates. Image (a) shows the particle before any SIMS analysis, (b) and (c) after several analyses in positive and negative modes. Each image is the sum of two images with two grazing incidence illuminations from the left and the right. Image (a) is a sub-pixel sampling, images (b) and (c) are nominal sampling (Langevin et al. 2016). The estimated height (Z) of the particle Atika is indicated for each image taken by the microscope COSISCOPE.

intensity peaks are at $m/z = 73.05$ [$Si(CH_3)_3^+$] and $m/z = 147.07$ [$Si_2O(CH_3)_5^+$]. Additional peaks from the target background include the primary ion $^{115}In^+$ at $m/z = 114.90$, the contribution of the gold target at $m/z = 196.97$ and some hydrocarbon fragments C_xH_y at $m/z < 100$.

The processing method to retrieve the signal coming from cometary particles in the positive mass spectra addresses three crucial points: the selection of relevant mass spectra, the choice of the normalization and the assessing of the so-called matrix effect that imposes a careful use of subtraction method when handling mass spectra.

For a given particle, the analysis is most of the time carried out as a line scan or a matrix. This allows covering a large area over the selected particle and next to it. It is therefore possible to obtain a substantial number of spectra over the particle plus some spectra over the background target. Several indicators allow sorting the mass spectra acquired on the particle (hereafter spectra ON) from those measured on the background near the particle (hereafter spectra OFF). The selection of the spectra ON is based on the COSISCOPE images, the low intensity of PDMS peaks (see the example of the particle Kenneth in Fig. 2), the high intensity of elemental ions such as iron ($^{56}Fe^+$) at $m/z = 55.94$ and magnesium ($^{24}Mg^+$) at $m/z = 23.99$, and the behaviour of $^{12}C^+$ ($m/z = 12.00$) becoming the most intense peak of the series C^+, CH^+, CH_2^+, CH_3^+ (Fray et al. 2016). The selection of the spectra OFF is mainly based on a high PDMS signal in comparison to the one on the particle (Fig. 2). Spectra have also been acquired on target plates before any exposure to the cometary dust; thus, they can be used as a background surface reference.

Mass spectra have to be normalized in order to be compared. The choice of the normalization can vary depending on the goal of the analysis. In this study, we have considered the PDMS peak intensity at $m/z = 73.05$ as the normalization parameter. The reason is that PDMS is the main contributor in the instrument background in the positive mass spectra and the peak at $m/z = 73.05$ is the highest one. The quantification of Si and C in the cometary particles is one of the main objectives of this study. In order to estimate these specific abundances, the contribution of PDMS to the signal of these elements has first to be removed as well as possible from the spectra ON.

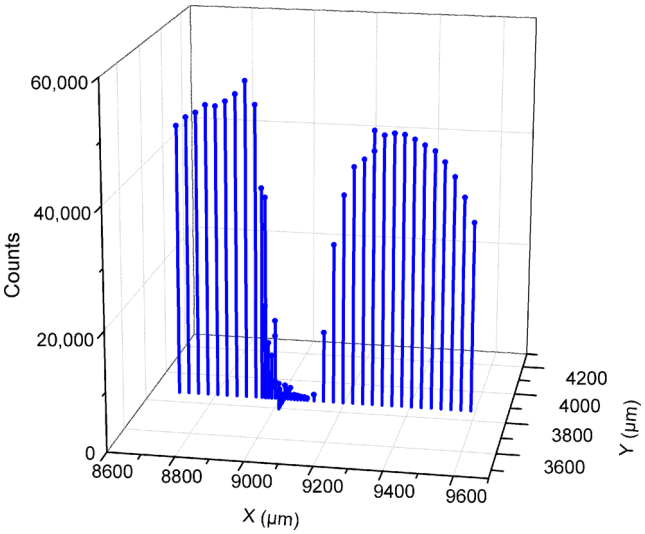


Figure 2. Spatial distribution of the PDMS intensity for the analysis of the particle Kenneth. The counts of the PDMS fragment $Si(CH_3)_3^+$ is displayed on (lowest values) and off (highest values) the particle.

The methodology to retrieve the signal coming from a cometary particle in the positive mass spectra is as follows (see Fig. 3 for illustrations of this methodology):

i. Selection of the spectra ON
ii. Selection of the spectra OFF
iii. For both sets of spectra ON and OFF, determination of the number of counts of the PDMS peak at $m/z = 73.05$
iv. Subtraction of the set of spectra OFF from the set of spectra ON after normalization to PDMS at $m/z = 73.05$. The cometary particle contribution to the peak intensity I_{E^+} is retrieved as follows:

$$I_{E^+} = I_{E^+_{ON}} - \left(I_{E^+_{OFF}} \times \frac{I_{PDMS^+_{ON}}}{I_{PDMS^+_{OFF}}} \right). \quad (1)$$

This work intends to report the global composition of 67P cometary particles. Besides the analysis of each particle individually, a total of 494 positive ions mass spectra ON from 25 distinct

Downloaded from https://academic.oup.com/mnras/article-abstract/469/Suppl_2/S712/4670835 by CNRS user on 04 June 2020

particles have been selected (see Table 1). This represents 247 different locations on the cometary particles, as for each analysis two successive spectra are acquired at the same *X*- and *Y*-coordinates. As explained below, in the results section, all the collected and analysed dust particles present similar mass spectra signatures. Thus, the sum of this large number of spectra allows increasing the signal-to-noise ratio to detect some elements that present a very low signal. An additional selection of 50 positive ion mass spectra acquired on the gold target plates before exposure to the cometary dust was used as the selection OFF.

Before calculations, the spectra are rebinned and mass calibrated. Then, a Levenberg–Marquardt algorithm (Denis & Schabel 1996) allows fitting the peaks by a Gaussian curve. The outcomes are the position, the width and the number of counts for each fitted peak. The residual of the peak fit is below 0.3 per cent. Normal isotopic abundances are considered (Lodders 2010) and mass interferences corrected (Stephan 2001). Background spectra display a $C^+/73^+$ ratio of about 0.01 due to contamination. For the analyses performed on the particles, spectra selected ON have a $C^+/73^+$ ratio at least 10 times larger than on the spectra OFF (extended data fig. 4 in Fray et al. (2016) for particle Kenneth with values ranging from 0.3 to 1.3). It implies that the carbon contribution of the contamination to the C^+ signal of the spectra ON Kenneth is below 3.3 per cent. For the sum of the 494 mass spectra, the contribution of the contamination to the C^+ signal is 5.4 ± 2.2 per cent and to the Si^+ signal it is 11.3 ± 3.4 per cent. After the subtraction of the contamination, the error on the estimation of the cometary C^+/Si^+ ratio is 5.6 per cent (2.2 per cent for C^+ + 3.4 per cent for Si^+). The same reasoning applies to the others element abundances determination in positive mode, except that these elements are nearly absent from the contamination.

Finally, we can compare the resulting background-subtracted spectra (initially presenting variable amounts of PDMS) with raw spectra taken on some particles presenting a very low level of background contribution. As an example, the sum of 30 positive ions mass spectra ON Atika is displayed in Fig. 3(a). It is an ideal case as the PDMS signal is nearly absent (i.e. the PDMS intensity at $m/z = 73.05$ is very low compared to the gold peak). As an illustration of the processing method, a selection of 4 mass spectra ON Umeka is displayed in Fig. 3(b). The spectrum clearly shows a major PDMS contribution in ON Umeka compared to ON Atika. Fig. 3(c) is the selection of 14 mass spectra OFF Umeka, showing a typical signature of the target background. Fig. 3(d) shows the result of the processing method to retrieve the cometary signal of Umeka, where the signals of PDMS at $m/z = 73.05$ and $m/z = 147.07$ are not present anymore. The processed spectrum is very similar to the raw spectrum of Atika on Fig. 3(a), particularly in that there is strong $^1H^+$, $^{12}C^+$ and $^{28}Si^+$ signals. This is the case for all cometary spectra processed (see also Fig. 5), independently of the intensity of PDMS peaks in the initial measured ON. The subtraction method described above allows to remove a large number of major background interfering peaks with the cometary particles' signatures. Some peaks after data post-processing still elude a proper characterization due to mass resolution, such as the one at $m/z = 43.00$ (Figs 3 and 5) with potential contribution of ions such as CH_3Si^+ ($m/z = 43.00$), $HNCO^+$ ($m/z = 43.01$) and $C_2H_3O^+$ ($m/z = 43.02$).

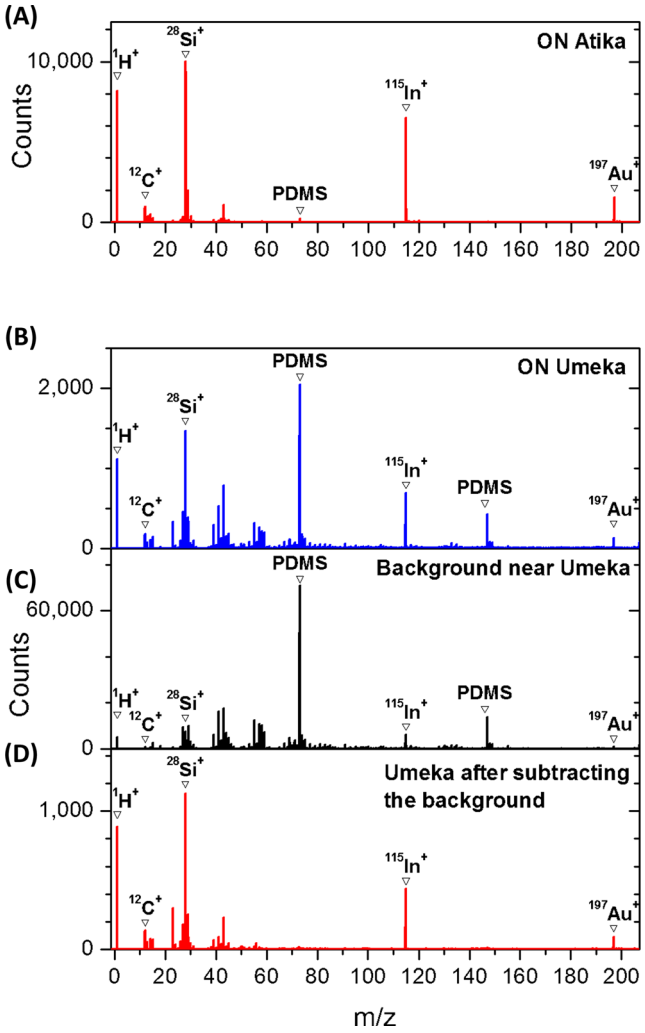


Figure 3. Application of the processing method to retrieve the cometary signal for the positive mass spectra. Image (a) displays the sum of 30 mass spectra ON Atika, (b) displays the sum of four mass spectra ON Umeka and (c) the sum of 14 mass spectra OFF Umeka. The mass spectrum displayed in (d) is the final signature of particle Umeka after the subtraction of its associated background.

2.4.2 Data analysis for negative mass spectra

In a typical negative ion mass spectrum of the target background, the PDMS signature is present with two main fragments at $m/z = 59.00$ (CH_3SiO^-) and $m/z = 74.99$ ($CH_3SiO_2^-$); however, PDMS is not the major contributor to the background signal. Other species, like halogen ions, are strongly present in the target signature, such as $^{19}F^-$ ($m/z = 18.97$), $^{35}Cl^-$ ($m/z = 34.97$), $^{37}Cl^-$($m/z = 36.97$), $^{79}Br^-$ ($m/z = 78.92$) and $^{81}Br^-$ ($m/z = 80.92$). The strong peak at $m/z = 196.97$ ($^{197}Au^-$) arises from the gold target plate.

The data treatment in negative mode has been handled by the use of a multivariate analysis namely the Non-negative Matrix Factorization (hereafter NMF) (Gillis & Vavasis 2014; Trindade, Abel & Watts 2017) that was particularly suitable for the COSIMA negative mode data. Here, we have used NMF to decompose the negative mode signal into two components, one corresponding to the background contribution and one corresponding to the cometary particles contribution. The signal S computed by NMF is described as follows:

$$S \cong (H_1 \times W_1) + (H_2 \times W_2). \quad (2)$$

Here W_1 and W_2 are the two spectral components; H_1 and H_2 are the weighting coefficients for each component. Before the NMF

Downloaded from https://academic.oup.com/mnras/article-abstract/469/Suppl_2/S712/4670835 by CNRS user on 04 June 2020

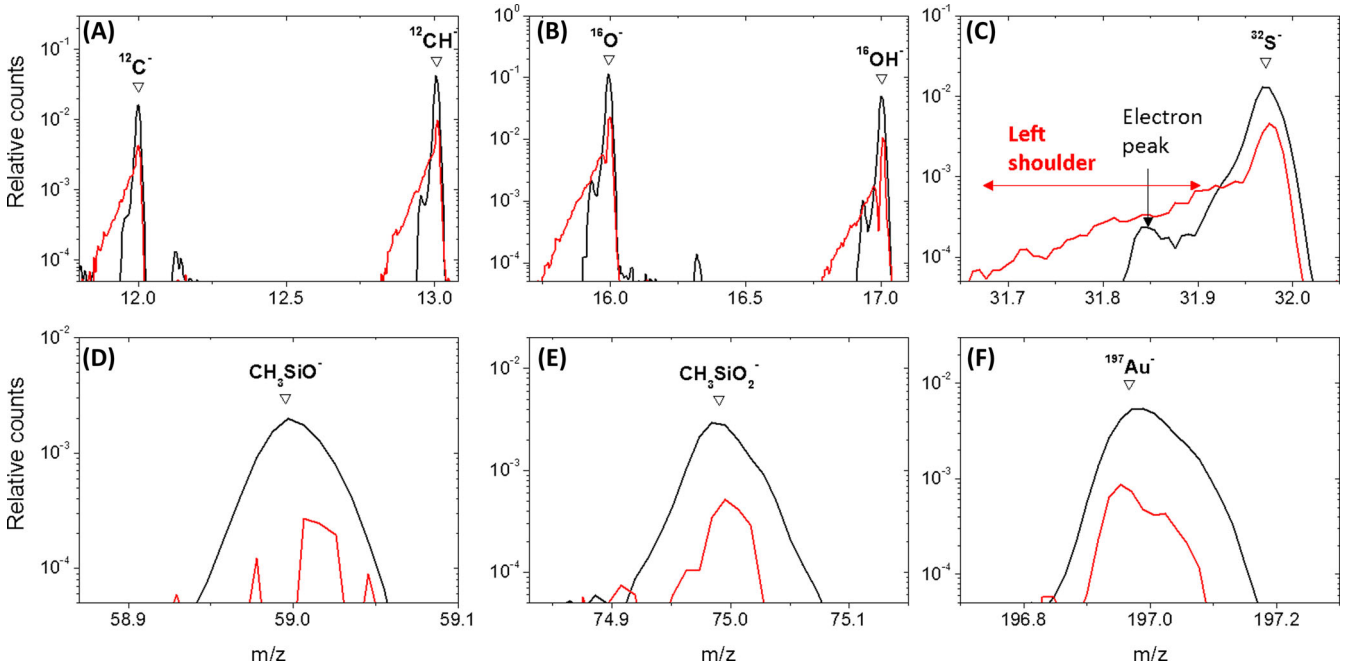


Figure 4. Application of the Non-negative Matrix Factorization (NMF) on a selection of negative mass spectra (target 1CF particles). The W_1 component (in black) is attributed to the background signature and the W_2 component (in red) to the cometary signature. For better visibility, the panels show the components W_1 and W_2 for specific mass ranges and a logarithmic scale for relative intensities.

method is applied, a careful selection of spectra taken ON and OFF the particles has to be performed, as for positive mode data treatment. When the NMF method is successfully applied, the W_1 and W_2 components correspond to two different looking spectra, W_1 is assigned to the background and W_2 to the cometary signature. In negative mode, we have been able to verify that both the NMF method and the normalization-subtraction method (applied similarly to what is described for positive mode) give similar results, in terms of mass spectra signatures and elementary quantifications. The NMF processing method can either be applied to single particles to reveal their individual signature, or to a set of particles to obtain an average signature.

In positive mode, specific peaks clearly arise only from the cometary particle. This is not the case in negative mode. However, a left shoulder next to the main peak systematically appears when a cometary particle contribution is accounted for, as displayed in Figs 4(a)–(c). This left shoulder differs from the electron peak (electrons sputtered off the grids within the reflectron are present in COSIMA negative ion spectra; Kissel et al. 2007). The left shoulder, observed in negative mode only, can be explained by the potential difference between the target plate and the surface of a particle that is due to the implantation of the positive primary ions $^{115}In^+$ in the insulating material of the particles. The negative ions ejected from a positively charged surface have then a lower velocity than those originating from the uncharged surface of the target. Due to the settings of the lenses in the reflectron of COSIMA, the ions originating from the charged surface (i.e. the cometary particles) have a shorter TOF than the ions from the uncharged surface (i.e. the background target) and hit the detector first (Fray et al. 2017; Hornung et al., in preparation).

An application of the data treatment for negative mass spectra is illustrated in Fig. 4. In this example, 38 spectra ON and 6 spectra OFF (acquired on the target plate 1CF) were selected and the NMF decomposition was applied to this selection. The two resulting components W_1 (in black) and W_2 (in red) are associated to the background signature and the cometary signature, respectively. The main peak preceded by a left shoulder is only present in the W_2 component for specific peaks corresponding to a signature from the analysed particle surface. In panel (a), this left shoulder is present in the cometary signature for $^{12}C^-$ ($m/z = 12.00$) and $^{12}CH^-$ ($m/z = 13.01$), in panel (b) for $^{16}O^-$ ($m/z = 15.99$) and $^{16}OH^-$ ($m/z = 17.00$) and in panel (c) for $^{32}S^-$ $m/z = 31.97$ (with a contribution from $^{16}O_2{}^-$ at $m/z = 31.99$). The principal peaks can contain a variable contribution from the target background. Two characteristic fragments of the PDMS are shown in panel (d) CH_3SiO^- ($m/z = 59.00$) and in panel (e) $CH_3SiO_2{}^-$ ($m/z = 74.99$). Another peak originating from the gold target, $^{197}Au^-$ ($m/z = 196.97$) is displayed in panel (f). These three peaks do not display a left shoulder and the near absence of PDMS and gold peaks in the W_2 component—the cometary signature—demonstrates the efficiency of the NMF decomposition. For accurate quantification results on the cometary particles content, we have only used the area of the shoulder peaks in W_2 component to assess ion relative ratios.

Interestingly enough, the average $^{12}C^-/^{28}Si^-$ ion ratio given by the left shoulder of the cometary particles signature is higher than the same ratio obtained from the background signature. Given that PDMS $[(C_2H_6OSi)_n]$ in the background spectra is the main contributor to $^{12}C^-$ and $^{28}Si^-$ peaks in negative mode, the C/Si atomic ratio is at least equal to 2 for the background. Therefore, a preliminary observation that can be made, according to negative mode measurements, is that the average C/Si cometary atomic ratio is necessarily above 2.

From this point onward, negative mode measurement will mainly be used to assess the O/Si atomic ratio in cometary particles. The NMF decomposition gives an error of about 10 per cent on the mean $^{16}O^-/^{28}Si^-$ cometary ion ratio. This uncertainty is due to the variability of the result depending on the selected set of spectra for each target.

Downloaded from https://academic.oup.com/mnras/article-abstract/469/Suppl_2/S712/4670835 by CNRS user on 04 June 2020

Table 2. RSF values used for elemental quantifications.

Element	RSF	(−)	(+)	Standard	Mode	COSIMA instrument
C/Si	0.025	0.005	0.007	Silicon carbide	Positive	Reference model
O/Si	12.2	1.1	1.1	Forsterite	Negative	Reference model
Na/Fe	18	12	35	(Krüger et al. 2015)	Positive	Reference model
Mg/Fe	1.6	0.8	1.6	Olivine San Carlos	Positive	Flight model
Al/Fe	1.8	1.1	2.8	(Krüger et al. 2015)	Positive	Reference model
Si/Fe	3.3	1.7	3.3	Olivine San Carlos	Positive	Flight model
K/Fe	27	13	24	(Krüger et al. 2015)	Positive	Reference model
Ca/Fe	3.9	1.7	3.0	(Krüger et al. 2015)	Positive	Reference model
Cr/Fe	1.5	0.6	0.9	(Krüger et al. 2015)	Positive	Reference model
Mn/Fe	2	0.3	0.4	(Krüger et al. 2015)	Positive	Reference model
Fe	$\equiv 1$			Olivine San Carlos	Positive	Flight model

2.5 Relative sensitivity factors

Quantification of elemental abundances in SIMS requires the use of relative sensitivity factors (RSFs). For a known element E relative to the normalizing element E_0, the RSF is calculated from a standard as follows:

$$\mathrm{RSF}\ \ (\mathrm{E},\ \mathrm{E_0}) = \frac{(I_{\mathrm{E}^\pm}/I_{\mathrm{E}_0^\pm})_{\mathrm{Standard}}}{(\mathrm{E}/\mathrm{E_0})_{\mathrm{Standard}}} \qquad (3)$$

$I_{\mathrm{E}^\pm}/I_{\mathrm{E}_0^\pm}$ is the ratio of the positive or negative secondary ion intensities and $\mathrm{E}/\mathrm{E_0}$ the elemental ratio of the standard.

Standards used to calculate an RSF have to be chosen carefully as the ionization yields depend on the sample material and the instrumental parameters. The RSFs deduced from calibration and used in this study to convert ion ratios to elemental ratios are presented in Table 2. As for the analyses conducted on the cometary particles, no sputtering was applied on the standards (Krüger et al. 2015). For most of the elements (Na, Al, K, Ca, Cr and Mn), the RSF values relative to Fe have been determined in positive mode by analyses of relevant minerals with the reference model (RM) of COSIMA (Krüger et al. 2015). Quantification of carbon with SIMS in this case is, however, challenging. In this study, the RSF (C, Si) has been measured from positive secondary ions of a silicon carbide (SiC) sample analysed in the RM instrument (≥97.5 per cent, Aldrich). Even though silicon carbide is not expected to be the main carrier of carbon in the cometary particles, it has been chosen as a proxy for an intimate mixture of C and Si at comparable abundance levels. The RSF (C, Si) extracted from the geometric mean value of the calibration measurements made on silicon carbide and the statistical 1-sigma error from these measurements are given in the Table 2. As a test, the RSF (C, Si) value was applied to the C^+/Si^+ ratio measured on the 50 positive ion mass spectra acquired on the gold target plates before their first exposure to the cometary dust. These spectra display a background signature largely dominated by PDMS $(C_2H_6OSi)_n$. The C/Si atomic ratio of $2.4^{+0.6}_{-0.5}$, calculated from the background spectra, is consistent with the PDMS average C/Si ratio of 2. Oxygen provides both O^- anions and O^+ cations; however, the O^+ signal is very weak in the positive mass spectra compared to the others peaks. On the contrary, the O^- peak has a very high number of counts in the negative mass spectra. Metals, such as Mg and Fe, produce only cations and thus cannot be used in the negative spectra as normalizing element. Silicon provides both cations and anions. In cometary dust, oxygen is expected to be essentially borne by silicates. A pure synthetic forsterite (Mg_2SiO_4) sample [provided by Centre de Sciences Nucléaires et de Sciences de la Matière (CSNSM), initially from A. Revcolevski], measured in the RM instrument in the negative mode, has been used to obtain the RSF (O, Si) in negative mode. The uncertainty is the statistical 1-sigma error calculated from different measurements on the forsterite sample. Thus, for carbon and oxygen, the RSFs given in Table 2 are relative to Si.

A terrestrial San Carlos olivine sample $[(Mg_{1.7}Fe_{0.2})SiO_4]$ of well-defined elemental abundances, provided by CSNSM, has been deposited on a gold target of the flight instrument (XM) before the launch of the spacecraft and stored in the instrument during the flight. This sample was repeatedly analysed by SIMS in space, under the same conditions as for the analyses of the cometary particles collected, and was used as an internal calibration to estimate RSF (Mg, Fe) and RSF (Si, Fe) for the cometary matter. The uncertainties of 50 per cent for these two RSFs take into account the measured variabilities within the COSIMA flight model olivine sample and the known variability of these RSFs among different mineral samples (Krüger et al. 2015).

3 RESULTS AND DISCUSSION

3.1 COSIMA mass spectra of 67P dust particles

The whole set of particles (>250) analysed by COSIMA between September 2014 and June 2016 present similar mass spectra signatures (in both negative and positive modes), which constitute a specific fingerprint for 67P's dust. Typical mass spectra of particles, measured in the positive mode by the COSIMA instrument, are presented in Fig. 5, after data post-processing. As shown in these spectra, a very high $^{28}Si^+$ peak is always accompanied by a strong $^{12}C^+$ signal, while peaks from other elements (e.g. $^{23}Na^+$, $^{24}Mg^+$, $^{56}Fe^+$) show varying intensities from one particle to another. This systematic signature has not changed over the 2 yr of the mission, and even if the observed variations reflect some compositional diversity among the particles, they are not correlated to their size, typology (Langevin et al. 2016), date of collection or time interval between collection and measurement. This signature indicates that at the scale of approximately 40 μm, which is the spatial resolution of the COSIMA ion beam, 67P dust particles are always a mixture of carbonaceous matter and mineral phases. This observation is consistent with the results from 1P/Halley dust analyses that have reported a mixture of 'CHON' and silicate components at sub-micrometre scales (Lawler & Brownlee 1992). It is also consistent with the analyses of cosmic dust particles of possible cometary origin collected on Earth, such as Chondritic Porous Interplanetary Dust Particles (CP-IDPs) and UltraCarbonaceous Antarctic MicroMeteorites (UCAMMs), which reveal chemical and mineralogical heterogeneity at the level of ∼100 nm and below (Bradley

Downloaded from https://academic.oup.com/mnras/article-abstract/469/Suppl_2/S712/4670835 by CNRS user on 04 June 2020

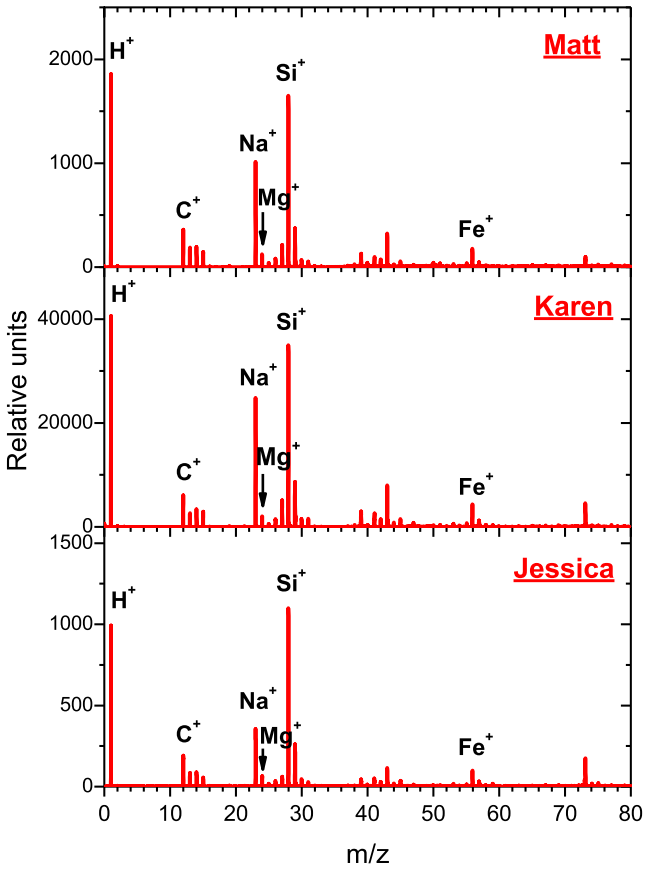


Figure 5. Typical positive ion mass spectra of three dust particles (Matt, Karen and Jessica) from comet 67P. The spectra are obtained after data post-processing and displays the major quantified elements C, Na, Mg, Si and Fe.

2010; Dobrică et al. 2012). This heterogeneity would thus be averaged at the scale of the COSIMA instrument analyses (∼35 × 50 μm^2).

3.2 Elemental composition of 67P's dust

In Table 3 is listed the average elemental composition relative to Fe of 67P's dust derived from the 30 particles selected for this study. The major elements quantified to date are C, N, O, Na, Mg, Si and Fe. Minor elements include Al, K, Ca, Cr and Mn. H and S are ubiquitous in the particles mass spectra, but their accurate quantification requires more ground calibration work. The N/Fe ratio shown in Table 3 is deduced from the N/C atomic ratio measured by Fray et al. (2017). These data complement and broaden the preliminary results acquired during the first 3 months of the mission at the comet (Schulz et al. 2015; Hilchenbach et al. 2016).

Fig. 6 displays the elemental abundances of the 67P particles calculated relatively to Fe [(E/Fe)$_{67P}$] and compared to the CI chondrite composition relatively to Fe (Lodders 2010). These results are compared to the *in situ* analyses of comet 1P/Halley inferred by PUMA-1 onboard Vega 1 (Jessberger et al. 1988) and to a compilation of laboratory analyses on 81P/Wild 2 dust particles captured in aerogel (Flynn et al. 2006; Ishii et al. 2008; Lanzirotti et al. 2008; Leroux et al. 2008; Stephan et al. 2008b). Our results show that the overall composition of 67P's dust, normalized to Fe, is chondritic within a factor of 3 for most of the elements. Nevertheless, a notable exception is constituted by C, which greatly exceeds the chondritic

Table 3. Elemental abundances relative to Fe in 67P's dust and in the CI-type chondrite (Lodders 2010).

Element	67P	(−)	(+)		
C/Si	5.5	1.2	1.4		
O/Si	5.5	0.5	0.5		
N/C	0.035	0.011	0.011		
Element	**67P**	**(−)**	**(+)**	**CI chondrite**	**(+/−)**
C/Fe	19	14	25	0.87	0.11
N/Fe	0.66	0.69	1.1	0.064	0.011
O/Fe	19	11	22	8.8	1.1
Na/Fe	0.28	0.18	0.56	0.07	0.01
Mg/Fe	0.40	0.20	0.40	1.2	0.1
Al/Fe	0.061	0.037	0.095	0.10	0.01
Si/Fe	3.5	1.7	3.7	1.1	0.1
K/Fe	0.0074	0.0035	0.0069	0.0042	0.0003
Ca/Fe	0.019	0.008	0.015	0.069	0.006
Cr/Fe	0.0093	0.0035	0.0062	0.015	0.001
Mn/Fe	0.015	0.003	0.003	0.011	0.001
Fe	≡ 1			≡ 1	

Note. The N/C atomic ratio has been measured by Fray et al. (2017). The uncertainties for 67P data are estimated from the RSFs. For the elements C, N and O, successive normalizations have been applied to obtain the abundances relative to Fe.

composition. As shown in Fig. 6, the composition of 67P's dust reported here is consistent with that of 1P/Halley and 81P/Wild 2. In the case of the latter, C, N, O and Si could not be quantified (Sandford et al. 2010; Brownlee 2014) and the high K amount is probably due to contamination (Stephan et al. 2008a).

3.3 The carbon and oxygen content

The average abundances of carbon and oxygen relative to silicon in 67P particles are shown in Fig. 7 and compared to the protosolar abundances (Lodders 2010) and to the compositions of Halley dust (Jessberger et al. 1988), CP-IDPs (Thomas et al. 1993) and CI chondrite (Lodders 2010). As mentioned before, for both these ratios, no data can be derived for 81P/Wild 2 dust. From Fig. 7(a), it can be noted that the high carbon-to-silicon atomic ratio in 67P's dust (C/Si = $5.5^{+1.4}_{-1.2}$) is close to the solar value and comparable to comet Halley's value. The C/Si ratio in 67P's dust is twice the value found on average in CP-IDPs [although in some single particles of anhydrous IDPs, carbon abundance is measured up to 47 wt% (Thomas, Keller & McKay 1996)] and six times higher than that in CI carbonaceous chondrites. However, it is much lower than what can be measured in some UCAMMs (C/Si atomic ratio higher than 50; Dartois et al. 2013). Fig. 8 presents the C/Si atomic ratio of the 67P cometary particles selected for positive mode analyses. It shows that the variability of the C/Si atomic ratio of the particles is not correlated to their collection target plate nor to their typology (Langevin et al. 2016). Fig. 9 shows that the ratio is also not correlated to their collection period, before or after the perihelion. As displayed in both figures, the C/Si ratios measured for the distinct particles span a fairly wide range (approximately from 2 to nearly 10, if we take the error bars into account), but they always remain distinctively high. This high C/Si ratio, close to the solar elemental abundance, may be an indication that these cometary dust particles have better preserved their initial semivolatile content than the primitive carbonaceous chondrites and CP-IDPs collected on Earth. Furthermore, as previously published (Fray et al. 2016), the carbon in 67P's dust particles is probably mainly present as

Downloaded from https://academic.oup.com/mnras/article-abstract/469/Suppl_2/S712/4670835 by CNRS user on 04 June 2020

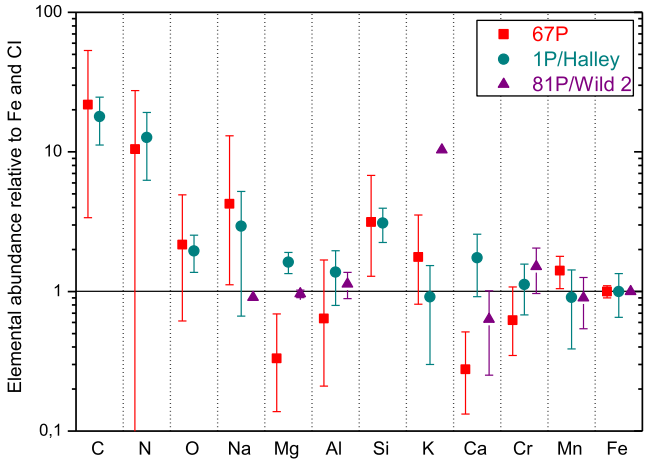


Figure 6. Comet 67P/Churyumov-Gerasimenko (67P) dust elemental ratios relative to Fe and to the CI chondrite composition (Lodders 2010) compared to 1P/Halley's dust (Jessberger et al. 1988) and 81P/Wild 2's dust collected in Stardust aerogel (Flynn et al. 2006; Ishii et al. 2008; Lanzirotti et al. 2008; Leroux et al. 2008; Stephan et al. 2008b). The values correspond to the relative ratios $(E/Fe)_{comet}/(E/Fe)_{CI}$. The N/C atomic ratio has been measured by Fray et al. (2017). The error bars for 67P data come from the RSFs' uncertainties and can be amplified by successive normalizations. For instance, the uncertainty displayed for C is the addition of uncertainty on the RSF for calculation of C/Si, plus uncertainty for Si/Fe, plus uncertainty on C/Fe in CI-type chondrite (see Table 3). Therefore, error bars can be 'artificially' enhanced due to successive normalizations to compare all elements on a same plot (this explains why error bars on N are so large in this plot, compared to the actual value measured for N/C, shown in Table 3).

macromolecular material, as it shows similarities with the Insoluble Organic Matter (IOM) found in carbonaceous chondrites. However, there are some differences, such as the inferred H/C ratio that is higher and could be indicative of a more primitive nature for 67P carbonaceous matter (Fray et al. 2016).

The lower O/Si atomic ratios of 67P and 1P/Halley dust, compared to that of the CI chondrites and to the protosolar values, are consistent with the pristine nature of these comets (Fig. 7b). Indeed, the high O/Si ratio in CI chondrites results from aqueous alteration of minerals in their parent body (Lodders 2010). The mass spectra of 67P dust particles do not show signatures indicating the presence of typical hydrated minerals, such as phyllosilicates, as evidenced by the very low OH^-/O^- ion ratio measured in 67P particles. Indeed, the OH^-/O^- ion ratio from the average composition of the selected particles ranges between 0.2 and 0.3, while for a phyllosilicate, the ratio is about 0.6 when measured on the reference model of COSIMA. The absence of signatures of hydrated minerals was also reported by the VIRTIS/*Rosetta* instrument (Capaccioni et al. 2015; Quirico et al. 2016). Compared to the protosolar abundance, the seeming lack of oxygen in 67P's dust could be due to the large amount of oxygen contained in water molecules, either in the gas or in the ice phases of the protosolar disc. Water, in these two forms, is not measured by COSIMA. These results underline a pristine mineralogy for the cometary material that has not undergone liquid water alteration, contrary to the CI chondrites.

3.4 Averaged composition of 67P's particles

Fig. 10 shows the mean elemental composition of 67P's particles in atomic (Fig. 10a) and mass (Fig. 10b) fractions. These results are based on the elements quantified in this work, the N/C atomic ratio measured by Fray et al. (2017) and on some reasonable assumptions detailed here after for H and S. We make the assumption that (i) H/C = 1. This ratio can be regarded as a reasonable estimate based on observations that the macromolecules detected in 67P's particles contain more H than the IOM measured in chondritic meteorites (Fray et al. 2016); the highest H/C in IOM being 0.8 (Alexander et al. 2007). Also, (ii) we assume that sulphur is mainly in iron sulphides, thus essentially bound to iron, and use a chondritic S/Fe atomic ratio of 0.5 (Lodders 2010). The mass ratio of organic to mineral matter in 67P's dust (Fig. 10c) was estimated with additional assumptions. (iii) The main carriers of the elements Si, Fe, Mg, Na, Al, Mn, Ca, Cr, K and S are supposed to be in the mineral phase. (iv) According to previous results (Fray et al. 2016; Fray et al. 2017), the main C and N carriers should be organic matter, whereas O is present in both organic and mineral phases. Considering the observations and elemental composition reported

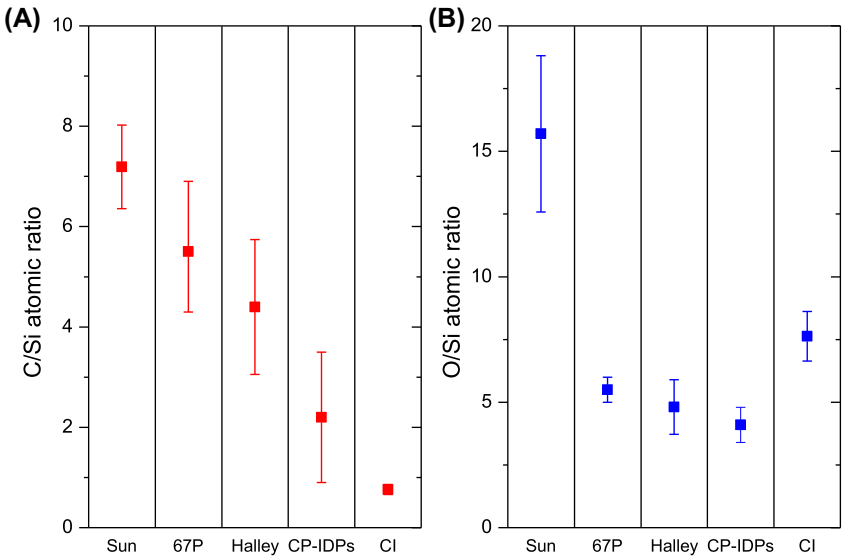


Figure 7. Comparison of (a) carbon and (b) oxygen elemental ratios relative to silicon in the protosolar disc (Sun) (Lodders 2010), cometary dusts of 67P (this work) and of Halley (Jessberger et al. 1988), CP-IDPs (Thomas et al. 1993) and CI chondrites (Lodders 2010).

Downloaded from https://academic.oup.com/mnras/article-abstract/469/Suppl_2/S712/4670835 by CNRS user on 04 June 2020

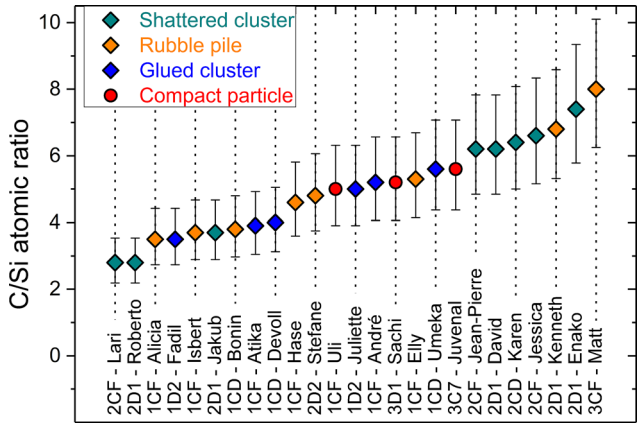


Figure 8. C/Si atomic ratio of the selected cometary particles. For each particle, the name, the collection target plate and the typology classification are indicated. The latter refers to the classification determined in Langevin et al. (2016). Data are obtained by the positive mode analyses and the error bars are calculated from the RSFs' uncertainties.

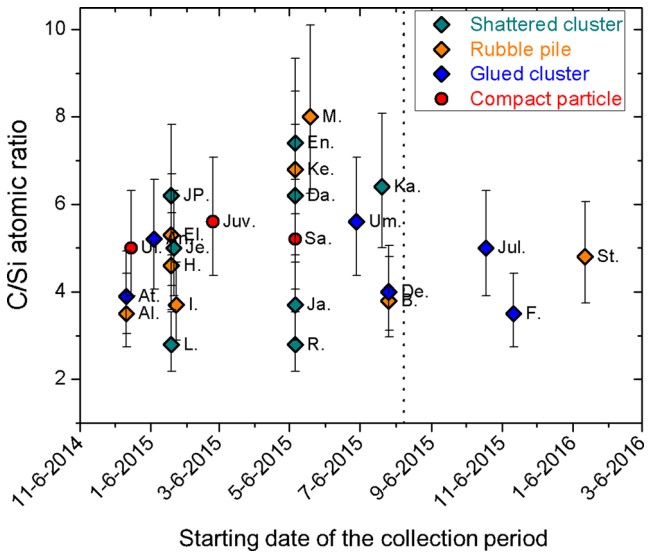


Figure 9. C/Si atomic ratio of the selected cometary particles as a function of their collection period. The typology of the particles refers to the classification determined in Langevin et al. (2016). Abbreviations of particle names are listed in Table 1. The dotted line represents the date of perihelion of comet 67P. Data are obtained by the positive mode analyses and the error bars are calculated from the RSFs' uncertainties.

in this study, the mineral phase in 67P's dust is predominantly composed of anhydrous silicates. Other oxides, if present, would be very minor phases. Then, (v) taking into account stoichiometry rules, the O/Si atomic ratio in the mineral phase would be, at most, 4. In that case, the remaining oxygen is in the organic phase and gives an assumed O/C atomic ratio of 0.3, which is close to the average O/C ratio of ~ 0.2 measured in the IOM of carbonaceous chondrites (Alexander et al. 2007), but lower than the O/C ~ 0.5 measured in a carbon-rich area of an anhydrous cluster IDP (Flynn et al. 2001). In conclusion, according to our results and these estimations, the carbonaceous content is approximately 45 per cent in mass in 67P dust particles of about 50–1000 μm in size.

This result also shows that the macromolecular carbonaceous matter, previously identified as being the main carbon-bearing component of dust particles (Fray et al. 2016), is one of the main constituents of the non-volatile components of comet 67P's nucleus. Considering the cometary volatile fraction, carbon-bearing compounds are observed by the ROSINA/*Rosetta* instrument at the level of a fraction of per cent in mass relative to water abundance (Le Roy et al. 2015), aside from CO_2 and CO which are the most abundant compounds in the coma after H_2O. If the dust-to-water mass ratio is above 5 in comet 67P (Fulle et al. 2016), by making a rough assumption that dust-to-ice ratio in the nucleus would be approximately the same, the macromolecular phase would be

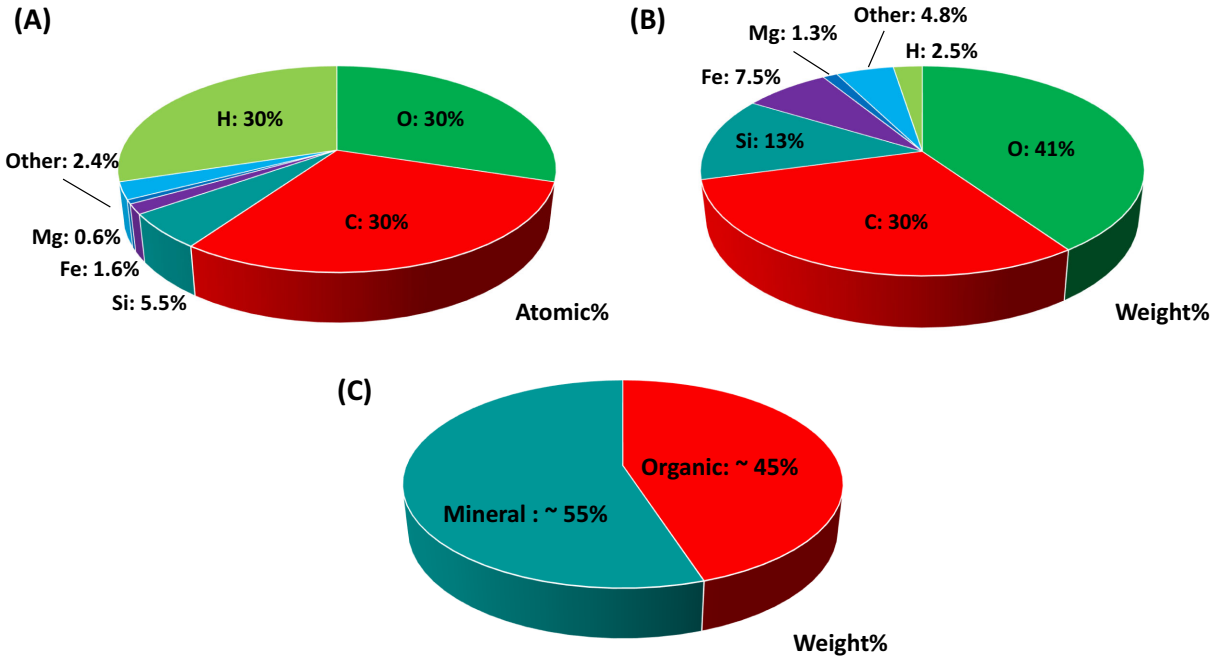


Figure 10. Averaged composition of 67P's dust particles as deduced from COSIMA measurements and some hypotheses detailed in the text. The averaged composition is given (a) by atomic fraction and (b) by atomic mass fraction. Image (c) is the mineral and organic content estimated in mass fraction.

Downloaded from https://academic.oup.com/mnras/article-abstract/469/Suppl_2/S712/4670835 by CNRS user on 04 June 2020

the main reservoir of carbon in the comet. Comets such as 67P and 1P/Halley being among the richest objects in carbon, the carbonaceous macromolecular phases could also be the main carbon reservoir in the early stage of the Solar System formation. Then, carbon has probably been delivered to Earth and other planets mainly under this macromolecular form, where it might have played a leading role in prebiotic evolution.

ACKNOWLEDGEMENTS

COSIMA was built by a consortium led by the Max-Planck-Institut für Extraterrestrische Physik, Garching, Germany, in collaboration with the Laboratoire de Physique et Chimie de l'Environnement et de l'Espace, Orléans, France; the Institut d'Astrophysique Spatiale, CNRS/Université Paris Sud, Orsay, France; the Finnish Meteorological Institute, Helsinki, Finland; the Universität Wuppertal, Wuppertal, Germany; von Hoerner und Sulger GmbH, Schwetzingen, Germany; the Universität der Bundeswehr, Neubiberg, Germany; the Institut für Physik, Forschungszentrum Seibersdorf, Seibersdorf, Austria; and the Institut für Weltraumforschung, Österreichische Akademie der Wissenschaften, Graz, Austria; and is led by the Max-Planck-Institut für Sonnensystemforschung, Göttingen, Germany. We acknowledge the support of the national funding agencies of Germany [Deutsches Zentrum für Luftund Raumfahrt (DLR), grant 50 QP 1302], France (Centre National d'Étude Spatiales, CNES), Austria, Finland and the European Space Agency (ESA) Technical Directorate. AB acknowledges support from the CNES and the Labex Exploration Spatiale des Environnements Planétaires (ESEP; no. 2011 LABX-030), and funding from the Idex Paris Sciences et Lettres (PSL; no. ANR-10-IDEX-0001-02). RI also acknowledges support from the Labex Exploration Spatiale des Environnements Planétaires (ESEP; no. 2011-LABX-030) and funding from the Idex Paris Sciences et Lettres (PSL; no. ANR-10-IDEX-0001-02). HL and BZ acknowledge Academy of Finland grant 277375. KV acknowledges support from the Austrian Science Fund (FWF), project P 26871-N20. We thank the *Rosetta* Science Ground Segment at the European Space Astronomy Centre, the *Rosetta* Mission Operations Centre at the European Space Operations Centre, and the *Rosetta* Project at the European Space Research and Technology Centre for their outstanding work enabling the science return of the *Rosetta* Mission. *Rosetta* is an ESA mission with contributions from its Member States and NASA.

REFERENCES

Alexander C. M. O., Fogel M., Yabuta H., Cody G. D., 2007, Geochim. Cosmochim. Acta, 71, 4380
Bell J. F., Davis D. R., Hartmann W. K., Gaffey M. J., 1989, in Binzel R. P., Gehrels T., Matthews M. S., eds, Asteroids II. Univ. Arizona Press, Tucson, AZ, p. 921
Bradley J., 2010, in Henning T., ed., Astromineralogy. Springer-Verlag, Berlin p. 259
Brownlee D., 2014, Annu. Rev. Earth Planet. Sci., 42, 179
Capaccioni F. et al., 2015, Science, 347, 4
Clark B. C., Mason L. W., Kissel J., 1987, A&A, 187, 779
Dartois E. et al., 2013, Icarus, 224, 243
Denis J. J. E., Schabel R. B., 1996, Soc. Ind. Appl. Math., 11, 431
Dobrică E., Engrand C., Leroux H., Rouzaud J. N., Duprat J., 2012, Geochim. Cosmochim. Acta, 76, 68
Flynn G., Feser M., Keller L. P., Jacobsen C., Wirick S., Avakians S., 2001, 32nd Annual Lunar and Planetary Science Conference. Houston, Texas, p. 1603
Flynn G. J. et al., 2006, Science, 314, 1731
Fray N. et al., 2016, Nature, 538, 72
Fray N. et al., 2017, MNRAS, 469, S506
Fulle M. et al., 2016, ApJ, 821, 19
Gillis N., Vavasis S. A., 2014, IEEE Trans. Pattern Anal. Mach. Intell., 36, 698
Henkel T., Gilmour J., 2014, in Turekian K. K., ed., Treatise on Geochemistry, 2nd edn. Elsevier, Oxford, p. 411
Hilchenbach M. et al., 2017, Phys. Eng. Sci., 375, 20160255
Hilchenbach M. et al., 2016, ApJ, 816, L32
Hornung K. et al., 2014, Planet. Space Sci., 103, 309
Hornung K. et al., 2016, Planet. Space Sci., 133, 63
Ishii H. A., Brennan S., Bradley J. P., Luening K., Ignatyev K., Pianetta P., 2008, Meteorit. Planet. Sci., 43, 215
Jessberger E. K., Christoforidis A., Kissel J., 1988, Nature, 332, 691
Kissel J. et al., 2007, Space Sci. Rev., 128, 823
Kissel J. et al., 1986a, Nature, 321, 336
Kissel J. et al., 1986b, Nature, 321, 280
Krüger H. et al., 2015, Planet. Space Sci., 117, 35
Langevin Y. et al., 2016, Icarus, 271, 76
Lanzirotti A., Sutton S. R., Flynn G. J., Newville M., Rao W., 2008, Meteorit. Planet. Sci., 43, 187
Lawler M. E., Brownlee D. E., 1992, Nature, 359, 810
Le Roy L. et al., 2015, A&A, 583, 12
Leroux H. et al., 2008, Meteorit. Planet. Sci., 43, 97
Lodders K., 2010, in Goswami A., Reddy B. E., eds, Principles and Perspectives in Cosmochemistry. Springer, Berlin-Verlag, p. 379
Merouane S. et al., 2017, MNRAS, 469, S459.
Mumma M. J., Charnley S. B., 2011, ARA&A, 49, 471
Quirico E. et al., 2016, Icarus, 272, 32
Rotundi A. et al., 2015, Science, 347, aaa3905
Sandford S. A. et al., 2010, Meteorit. Planet. Sci., 45, 406
Schulz R. et al., 2015, Nature, 518, 216
Stephan T., 2001, Planet. Space Sci., 49, 859
Stephan T., Flynn G. J., Sandford S. A., Zolensky M. E., 2008a, Meteorit. Planet. Sci., 43, 285
Stephan T. et al., 2008b, Meteorit. Planet. Sci., 43, 233
Thomas K. L., Blanford G. E., Keller L. P., Klöck W., McKay D. S., 1993, Geochim. Cosmochim. Acta, 57, 1551
Thomas K. L., Keller L. P., McKay D. S., 1996, in Gustafson Bo A. S., eds, Hanner Martha S., Astron. Soc. Pacific, San Francisco, p.283
Trindade G. F., Abel M.-L., Watts J. F., 2017, Chemometr. Intell. Lab. Syst., 163, 76
Willacy K. et al., 2015, Space Sci. Rev., 197, 151

This paper has been typeset from a Microsoft Word file prepared by the author.

Downloaded from https://academic.oup.com/mnras/article-abstract/469/Suppl_2/S712/4670835 by CNRS user on 04 June 2020